Neutron spectra from beam-target reactions in dense Z-pinches

B. Appelbe and J. Chittenden

Citation: Physics of Plasmas **22**, 102703 (2015); doi: 10.1063/1.4933117
View online: http://dx.doi.org/10.1063/1.4933117
View Table of Contents: http://scitation.aip.org/content/aip/journal/pop/22/10?ver=pdfcov
Published by the AIP Publishing

Neutron spectra from beam-target reactions in dense Z-pinches

B. Appelbe[a] and J. Chittenden
Centre for Inertial Fusion Studies, The Blackett Laboratory, Imperial College London, London SW7 2AZ, United Kingdom

(Received 2 June 2015; accepted 29 September 2015; published online 13 October 2015)

The energy spectrum of neutrons emitted by a range of deuterium and deuterium-tritium Z-pinch devices is investigated computationally using a hybrid kinetic-MHD model. 3D MHD simulations are used to model the implosion, stagnation, and break-up of dense plasma focus devices at currents of 70 kA, 500 kA, and 2 MA and also a 15 MA gas puff. Instabilities in the MHD simulations generate large electric and magnetic fields, which accelerate ions during the stagnation and break-up phases. A kinetic model is used to calculate the trajectories of these ions and the neutron spectra produced due to the interaction of these ions with the background plasma. It is found that these beam-target neutron spectra are sensitive to the electric and magnetic fields at stagnation resulting in significant differences in the spectra emitted by each device. Most notably, magnetization of the accelerated ions causes the beam-target spectra to be isotropic for the gas puff simulations. It is also shown that beam-target spectra can have a peak intensity located at a lower energy than the peak intensity of a thermonuclear spectrum. A number of other differences in the shapes of beam-target and thermonuclear spectra are also observed for each device. Finally, significant differences between the shapes of beam-target DD and DT neutron spectra, due to differences in the reaction cross-sections, are illustrated. © *2015 AIP Publishing LLC*. [http://dx.doi.org/10.1063/1.4933117]

I. INTRODUCTION

The study of neutron production in Z-pinches dates back to the 1950s.[1] Much of this history concerns work to develop deuterium Z-pinches as a fusion energy source, and so the distinction between a hot, thermonuclear (TN) plasma and a beam-target (BT) plasma in which the bulk plasma was relatively cold was crucial. More recently, the deuterium dense plasma focus (DPF) has been developed as a reliable source of MeV neutrons.[2] In this application, BT neutron production is an acceptable mechanism as long as specifications such as yield and reliability are met. However, meeting these specifications is difficult without a detailed knowledge of the micro-physics of the Z-pinch. Most notably, the yield scaling with current does not agree with basic theory.[2,3] Furthermore, experimental[4,5] and computational[6] work have previously indicated that TN neutron production becomes significant for currents greater than 10 MA. However, the transition from BT to TN production is poorly understood. In this paper, we show that neutron energy spectra from BT reactions can have a number of characteristic shapes depending on the conditions in the stagnated Z-pinch. The aim of the paper is to improve our understanding of how neutron spectroscopy can be used as a diagnostic in Z-pinches.

We use a hybrid 3D MHD-kinetic model to simulate a number of DPF and gas puff devices. The plasma dynamics during the radial and pinch phases of a DPF implosion is similar to those of the gas puff, which suggests that a unified approach to modeling the devices would be beneficial.[7] The model predicts distinct features in the neutron spectra for the different devices. Some of these features are qualitatively similar to neutron spectra that have been observed in experiments.

The particular physical processes that we are interested in are (1) the growth of instabilities during the implosion phase of a dense Z-pinch leading to a perturbed pinch at stagnation and its turbulent break-up, (2) the generation of large electromagnetic fields that cause ions to be accelerated in a non-thermal manner during stagnation and break-up, and (3) neutron production from BT reactions between the accelerated ions and the background plasma.

These physical processes were first identified by Anderson *et al.*[1] in a study of deuterium pinches in discharge tubes. An unexpectedly high neutron yield was explained by the growth of an $m = 0$ instability that generated an electric field (**E**), which axially accelerated deuterium ions to an average energy of 50 keV. This deuteron energy was inferred from the measurement of neutron energies in both axial directions. Interestingly, it was suggested that magnetization of the accelerated ions could explain the relatively wide neutron distributions measured, but this could not be verified.

Computational modeling of the BT process was advanced by the introduction of a "generalized beam-target model" in which accelerated ions were assumed to have a wide angular and energy distributions.[8] Such models allowed the effects of magnetic field (**B**) to be included and provided good fits with experimental data.[9] However, the ion distributions in these models were initialised in an arbitrary manner, with little relation to the structure of the pinch at stagnation.

The initial formation of the ion beam remains poorly understood,[10,11] partly due to the difficulty in observing it in experiments. A wide variety of mechanisms have been suggested including Fermi acceleration,[12] finite Larmor radius effects,[13] and increased anomalous resistivity due to the

[a]Electronic mail: b.appelbe07@imperial.ac.uk

lower hybrid drift instability.[14,15] The most commonly cited mechanism is the large **E** field induced during the growth of Rayleigh-Taylor instabilities. This mechanism has been identified as the cause of BT neutrons in Particle-in-Cell (PIC) simulations of dense Z-pinches.[6,16] However, a lot of uncertainty remains about this acceleration mechanism including its dependence on instability growth rate, current, and plasma density. Whilst we do not rule out other mechanisms as contributing to neutron production in Z-pinches, we focus on this mechanism as it is thought to be strongly influenced by the MHD instabilities in a stagnated pinch. The approach that we take to model it is discussed in Sec. II B.

There is a vast literature on experimental work on neutron producing DPFs and gas puffs.[2] Of particular interest to us is the work in which neutron energy spectra have been reported. In Sec. IV, we mention a number of references in which neutron spectra with features similar to the spectra simulated here were reported. We also note that it is common in the experimental literature to use anisotropy of the neutron yield as a signature of BT neutron production.[17–19] Less frequently, isotropy of the neutron yield has been used to infer a TN source.[20] However, in this work, we show that it is possible to get an isotropic neutron yield and spectra from a BT source due to magnetization of the accelerated ions.

In conclusion, there is a long history of study of BT neutron production in Z-pinches. What is novel about the work that we present here is that we carry out 3D simulations of the full implosion of the device, from current initiation onwards. In addition, we focus on the shape of neutron spectra and identify some key features that can be used for diagnostic purposes.

The paper is organised as follows: Section II describes the computational models that have been used in this study. Section III describes the results of simulations for 3 different devices. Section IV discusses the important features that were observed in the calculated neutron spectra and the potential for using these features as a diagnostic. Finally, Sec. V summarizes the main points of this paper.

II. DESCRIPTION OF THE MODELS USED

The simulations reported here achieve two goals. The first goal is to understand the implosion dynamics and stagnation phase of gas puffs and DPFs. This is best achieved using a 3D MHD model in which the growth of instabilities is well represented, resulting in a stagnation phase that contains an inhomogeneous, turbulent, dense plasma. The second goal is to understand how the electromagnetic field structure present during the stagnation phase affects ion acceleration, transport, and subsequent neutron production. Since ion acceleration and transport is a kinetic process, we use a hybrid model to represent this in which a small fraction of the plasma ions are converted into computational PIC particles that are transported through the background MHD simulation. Reactions between these PIC particles and the background plasma result in BT neutrons. The important features of the models used are described in greater detail in Subsections II A–II C.

It should be noted that PIC simulations of both gas puffs and DPFs have previously been carried out.[14,21] Unlike PIC simulations, the hybrid model that we use here is not fully self-consistent since ions are treated as tracker particles that do not contribute to the background electromagnetic fields. However, the model is justified because 3D MHD simulations give a very good representation of the implosion and stagnation of the pinch and the accompanying growth of perturbations.[22] Realistic instability growth in 3D is difficult to achieve with a PIC code. Furthermore, the relatively low number of accelerated particles makes the tracker particle assumption reasonable.

A. MHD simulations

We use the Gorgon code for the MHD simulations.[23] This is a 3D Eulerian MHD code that uses the single fluid approximation but with separate ion and electron temperatures. Braginskii transport coefficients for heat conductivity κ and resistivity η. Blackbody radiation losses are accounted for and it is assumed that the plasma is optically thin. A fixed current waveform of the form $\frac{1}{2}I_{max}\left(1-\cos\left(\pi\frac{t}{\tau}\right)\right)$ is applied to the system, where τ is the current rise-time are used.

An important feature of the MHD simulation is the growth of instabilities during the implosion phase leading to a stagnated plasma that is inhomogeneous and turbulent. A 3D MHD simulation is required to model the $m=1$-type instability of the plasma as it breaks apart. In order to model instability growth, it is necessary to seed the initial system with a perturbation. In the case of gas puff simulations, perturbations of the mass profile of the gas jets are included.[4] In the case of DPFs, perturbations may arise due to differences in the breakdown times between the anode and different cathode rods. Simulation of this breakdown process would require detailed modeling of electron-neutral collisions and insulator surface effects that are beyond the scope of the current MHD model. Therefore, in order to initialise a perturbation in the rundown phase, narrow plasma channels from the anode to each cathode rod at the base of the DPF are preheated with a random temperature of ≤ 1 eV. This provides a preferential path for the current to initially flow through. The channels with higher temperature have a lower resistivity, and so the plasma tends to be accelerated from these regions earlier in time than from colder channels. The upper bound value of 1 eV was chosen such that a preheated channel reached a height of not greater than 2 mm when a channel without preheating begins to lift off the base.

The turbulent plasma at stagnation is accompanied by highly perturbed **E** and **B** fields. The electric field is given by $\mathbf{E}=\eta\mathbf{j}-\mathbf{v}\times\mathbf{B}$, where η is resistivity and **v** is the plasma velocity. Nominal values of the **E** field at stagnation in the different devices simulated are given in Sec. III. For a uniform, unperturbed, imploding Z-pinch **v** is radial, **B** is azimuthal and **j** and **E** are always in the axial direction. However, in a perturbed implosion, plasma can flow in a non-radial direction due to instabilities and the current path can be non-axial. This results in perturbations of the **E** field and, in particular, there are regions in which a large **E** field is directed outwards from the plasma surface into the vacuum.

Non-thermal acceleration of ions can occur at such locations, as discussed in Sec. II B.

B. Ion beam formation and transport

Data for the ion and electron temperatures, plasma density, and **E** and **B** fields are outputted at regular intervals during the stagnation phase of the MHD simulation. These data are post-processed to create computational particles representing ions that can be freely accelerated by the **E** field.

The algorithm for creating particles is based on identifying regions of the MHD plasma in which the **E** field can accelerate ions from dense plasma into a low density or vacuum region. These conditions are met mainly during the post-stagnation, turbulent break-up of the pinch when very strong **E** fields that are directed orthogonally to the plasma surface can arise. For each computational cell, the algorithm calculates the dot product of **E** field vector and $\nabla\rho$ (ρ is plasma density). If this quantity is negative, then the **E** field will accelerate ions from regions of higher to lower density and ions with a low collisionality (located in the high-energy tail of the Maxwellian distribution) will enter the kinetic regime. It was found that, by setting the fraction of ions accelerated from the tail to be that for which the acceleration due to the **E** field is greater than the deceleration due to collisions, the resulting yield of BT neutrons was in agreement with experimental data for a 70 kA DPF in which the TN yield was negligible. Therefore, the same model was used for ion acceleration in other devices modeled.

We refer to this mechanism for ion acceleration as a weak runaway model as there is no feedback from the kinetic model to the MHD model. It is also assumed that the MHD plasma remains quasi-neutral after the creation of kinetic ion particles and so kinetic electrons and repopulation of the tail of the ion Maxwellian distribution are not modeled. While both of these assumptions may be justified by the fact that only a small fraction of the MHD plasma is converted to kinetic particles, it is possible that accelerated ions will affect the evolution of the electromagnetic fields during stagnation, particularly in the localised regions in which the particles are created, while tail repopulation may affect the production rate of kinetic ions.

Typically, 100 computational particles are created per cell per time-step. These particles are weighted to account for the number of ions that are estimated to runaway from that cell. The Lorentz equation for these particles is solved and their motion through the system is tracked. The time-step for the particles is chosen such that the gyro-motion of the particles is resolved. Existing particles continue to evolve in the system when the MHD data are updated and new particles are created.

As the particles move through the system, they undergo two types of interaction with the background plasma. These are Coulomb collisions with both the background ions and electrons and nuclear reactions with the background ions. The second of these interactions is discussed in Subsection II C. Coulomb collisions are modeled using dynamic friction and diffusion coefficients in velocity-space that are a function of the particle's velocity.[24] In the simulations reported here, it is found that, in general, Coulomb collisions have only a small effect on the evolution of the computational particle momentum, which is dominated by the **E** and **B** fields. Coulomb collisions between computational particles are also modeled, but these have a very small effect due to the low density of beam ions.

We note that the ion beam formation and acceleration mechanism that we have just described model a specific physical process. Other sources of high energy ions may be present in a stagnated Z-pinch, such as those described in Section I. A more rigorous transition from MHD plasma to kinetic ions that takes into account a wider range of kinetic effects is currently under investigation.[25]

C. Calculating neutron yields and spectra

We distinguish between two different neutron producing processes taking place in the plasma. These are TN neutron production and BT neutron production. We do not calculate neutron production due to beam-beam particle interactions. Such a source of neutrons will be low due to the low density of beam particles in the simulations.

The neutron yield from the TN process can be calculated directly in the MHD part of the simulation as it is a function of ion temperature and density only. The shape of the TN neutron spectrum emitted at a given time is a function of the instantaneous ion temperature, density, and the bulk fluid velocity of the plasma.[26] A bulk fluid velocity that is sufficiently large (approximately $10^4\,\mathrm{ms}^{-1}$ or greater) can cause a shift in the spectrum of emitted neutrons. As discussed in Section IV B, it is thought that this effect can cause anomalous broadening of TN spectra. Therefore, we calculate TN spectra with the fluid velocity given by the MHD simulation and also with the fluid velocity set to zero. This provides a way to estimate the effect of anomalous fluid motion broadening of the TN spectra, which does not alter the TN yield. The procedure for calculating the spectra is as follows: In our simulations, at each time-step of the MHD simulation, the square of the plasma density of a computational cell multiplied by the time-step ($\Delta t n_f^2$, where Δt is the time-step size and n_f is the plasma density) is binned according to the ion temperature, fluid velocity magnitude, and fluid velocity direction relative to a specified detector location. A separate neutron spectrum can then be calculated for each element of the bin and is weighted according to the value of that bin element. The resulting spectra are summed to give a composite spectrum that represents the time-integrated TN neutron spectrum from the plasma.

A similar binning method is used for calculating the neutron yield and energy spectra from BT reactions. As the accelerated ions move through the background MHD plasma, the time-integrated reactivity of the ions with the background plasma can be calculated.[27] The weighting of the computational particle is reduced accordingly, and a running total for the time-integrated reactivity of all particles gives the neutron yield. For the BT neutron spectrum, the quantity $\Delta t n_b n_f$, where Δt is the time-step size, n_b is the beam particle density, and n_f is the background plasma

density, is binned according to background plasma ion temperature, beam particle energy, and the angle between the beam particle momentum direction and the vector towards the detector. For each bin element, a neutron spectrum can be calculated using a previously derived integral expression.[28] This model takes into account the effect of thermal broadening on the emitted spectrum. This is generally small relative to the broadening that arises from the wide spread of beam energies. However, it is important to model the thermal broadening effect correctly as it is anisotropic, and the simulated spectra contain evidence of it.

Cross-sectional data for the $D(d,n)He^3$ and $D(t,n)He^4$ reactions are taken from the ENDF database.[29] Examples of the cross-sectional data are shown in Fig. 1 for energies that are relevant to our study of ions accelerated in stagnated Z-pinches. We note that the total cross-section for the $D(t,n)He^4$ has a maximum value at a projectile energy of approximately 100 keV, while the $D(d,n)He^3$ increases monotonically with increasing temperature. Therefore, the BT neutron spectrum in a DT plasma will be most strongly influenced by ions with energies less than a few 100 keV even if ions are accelerated to much higher energies in the system. However, the BT neutron spectrum from a DD plasma will give a better representation of the highest energy reached by the accelerated ions. Figure 1 also shows that the differential cross-sections for the reactions are strongly anisotropic, and this needs to be accounted for when calculating the neutron spectra.

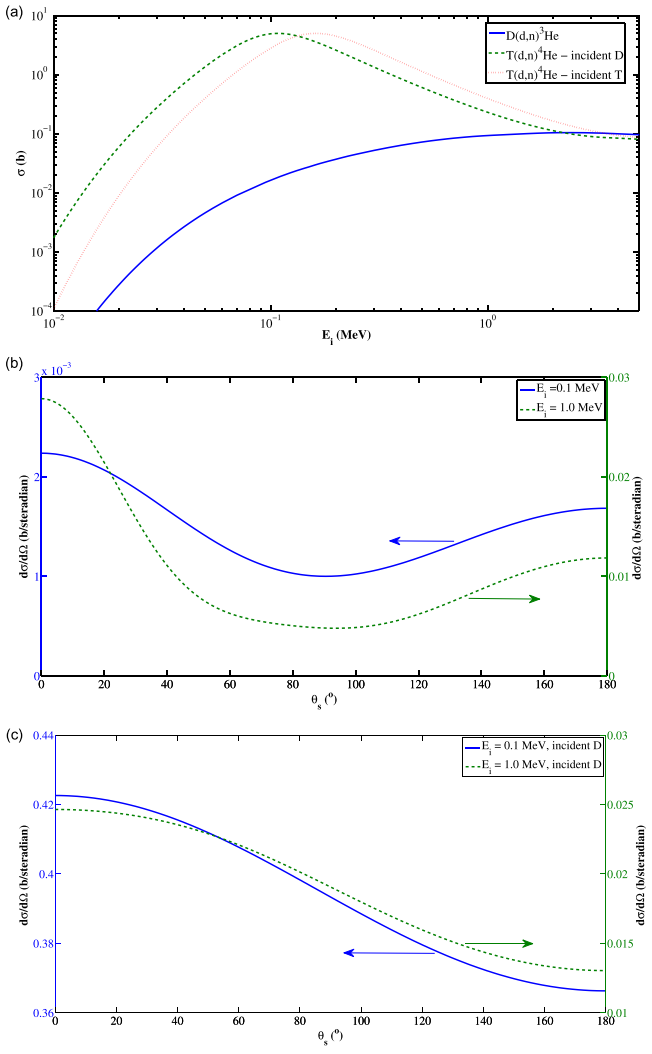

FIG. 1. Top: Total cross-section for $D(d,n)He^3$ and $T(d,n)He^4$ as a function of incident particle energy E_i (assuming other reactant particle is stationary). Middle: Differential cross-section for $D(d,n)He^3$ as a function of angle between incident particle and emitted neutron for two different incident particle energies. Bottom: Differential cross-section for $T(d,n)He^4$ for two values of incident deuteron energy (triton is stationary).

The neutron yield from BT reactions is strongly dependent on the number of beam ions that are present in the system. The only source of beam ions in our model is the weak runaway condition and so calculated neutron yields may be susceptible to the modeling uncertainties discussed in Section II B. However, the shapes of the neutron spectra are insensitive to the conditions in the regions where ions are initially accelerated. This is because the ions undergo significant nonlocal transport before reacting. Therefore, the neutron spectra shapes are dominated by the large-scale **E** and **B** field topologies generated by the turbulent pinch.

III. SIMULATION RESULTS

In this section, we report results for the simulations of a gas puff and two different types of DPF. In each case, we are particularly interested in the neutron spectra resulting from BT reactions. These spectra show different characteristics for each device, which can be understood in terms of the differing properties of the imploding Z-pinch. In particular, the dynamics of the accelerated ions in each device is strongly dependent on both the strength and topology of the **E** and **B** fields at stagnation.

A. 15 MA gas puff

Deuterium gas puff experiments on the Z machine produced 3×10^{13} neutrons.[4,30] The gas puff consisted of two annular shells of deuterium, spanning radii of 1–2 cm and 3–4 cm, approximately 2 cm in height and with a total linear mass of 405 μg cm^{-1}. The maximum current in the experiments was 15.4 MA. Neutron diagnostics used included indium activation detectors in both radial and axial directions and neutron time-of-flight (nTOF) detectors. The activation detectors indicated that the neutron yield was isotropic, while the nTOF detectors measured mean neutron energies of 2.34±0.1 MeV and 2.09±0.2 MeV in the radial and axial directions, respectively (a spectrum width was not reported). In addition to these experimental data, MHD simulations[4] and theoretical arguments suggested that the majority of the neutrons were produced by a TN mechanism. In this work, we simulate the gas puff experiments in order to estimate the BT yield and identify potential signatures of BT neutron production in neutron spectra.

The MHD simulation shows that at peak compression, the plasma density reaches 0.007 g cm^{-3} with an ion temperature of over 10 keV in the dense plasma column. The hybrid kinetic model begins 90 ns after the start of the simulation, when peak compression is reached. The kinetic model then runs for 10 ns during which time the stagnated column begins to break-up. The MHD data used in the kinetic model are

updated every 2 ns during this period. Whilst a shorter time interval for this update would be preferable, the MHD plasma is evolving slowly and so there is no significant change in the electromagnetic field structure during a 2 ns interval. Approximately 10^5 computational particles are created at the beginning of each interval. The **E** field reaches a maximum value of $5 \times 10^9\,\mathrm{V\,m^{-1}}$ in the vacuum region between Rayleigh-Taylor spikes and has a value of over $10^8\,\mathrm{V\,m^{-1}}$ near the plasma surface in the region where ions are accelerated. The **B** field has a peak value of over 10^3 T near the stagnated plasma column and maintains a mean value of approximately 500 T in low plasma density regions for the duration of the stagnation period. The MHD simulations produce a TN neutron yield of 4×10^{13} neutrons, in close agreement with the experiment ($4 \times 10^{13} \pm 20\%$), while the hybrid kinetic model produces a BT yield of 10^{12} neutrons.

The neutron spectra from the simulation are shown in Figs. 2 and 3. The time-integrated TN spectrum is shown in Fig. 2 both with and without the effects of fluid motion. Fluid motion causes a broadening and anisotropy of the TN spectra. Ion temperatures can be inferred from the FWHM of the TN spectra.[26] For the spectrum without fluid motion, the inferred ion temperature is approximately 6.1 keV, while the mean ion temperature inferred from the widths of the TN spectra with fluid motion is approximately 7.1 keV.

In Fig. 3, the time-integrated BT spectra at 5 ns and 10 ns after the onset of stagnation are shown. The BT spectra are significantly wider than the TN spectrum. The other notable features of the BT spectra are the degree of isotropy, the spectra peaks located at an energy of less than 2.45 MeV, and the long high energy tail extending beyond 4 MeV. These features are particularly obvious in the time-integrated spectra after 10 ns. The dynamics of accelerated ions can help to explain these features. A number of trajectories of accelerated ions are shown in Fig. 4 for the gas puff. Gyro-motion of the ions due to the **B** field is clearly present. Rather than moving axially, these ions are trapped by the azimuthal **B** field. This has the effect of causing beam ions to move isotropically rather than being preferentially accelerated in one direction, even though the electric field is primarily in the axial direction. Furthermore, Fig. 5 shows the evolution of energy as a function of time for two beam

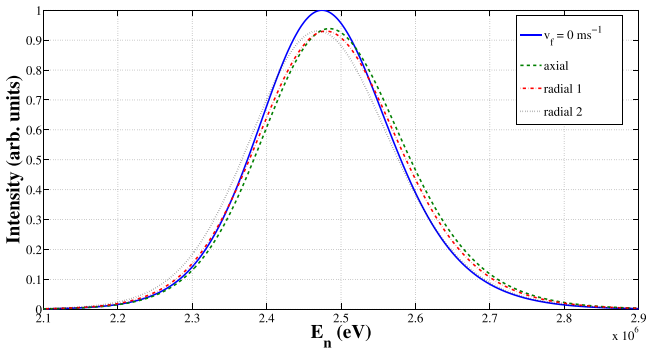

FIG. 2. The time-integrated TN spectrum for a deuterium gas puff without fluid motion broadening ($v_f = 0\,\mathrm{ms^{-1}}$) and with fluid motion broadening for emission in 3 different directions. The $v_f = 0\,\mathrm{ms^{-1}}$ spectrum has a FWHM of 206 keV, while the mean width of the spectra with fluid motion broadening is 222 keV.

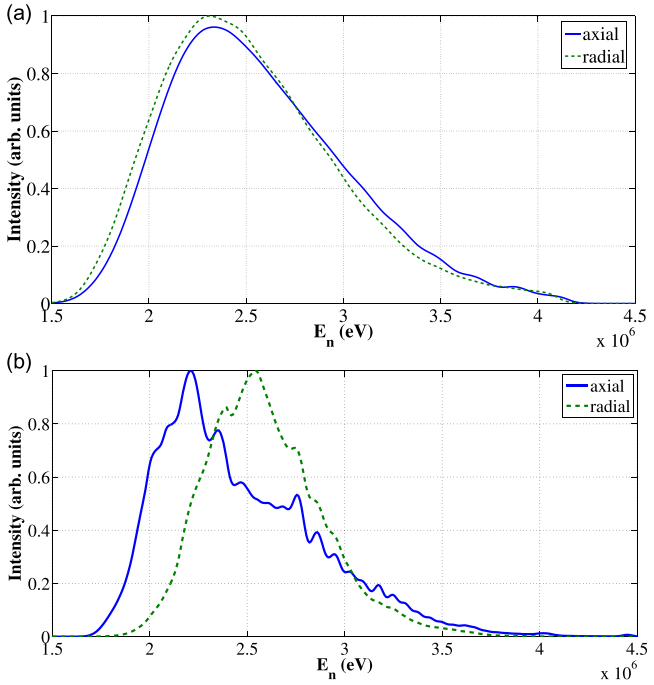

FIG. 3. Time-integrated BT spectra in the radial and axial directions for a deuterium gas puff at 5 ns (top) and 10 ns (bottom) after the onset of stagnation.

particles. These particles oscillate through energy ranges of several hundreds of keV during the stagnation period. This occurs because the particles are both magnetically confined and subject to a large orthogonal **E** field, which accelerates ions for one half cycle of the gyro-motion and decelerates the particles for the other half cycle. The effect that this gyro-motion in an $\mathbf{E} \times \mathbf{B}$ field has on a BT neutron spectrum is shown in Fig. 6. For a 500 keV deuteron, the energy of a

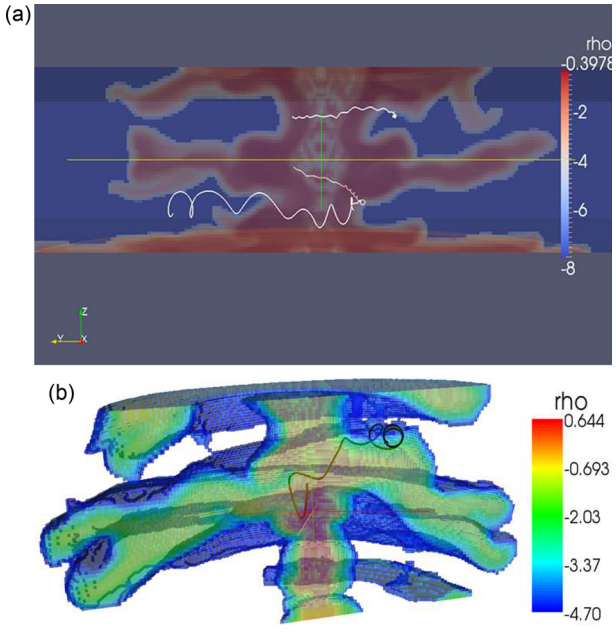

FIG. 4. Top: The trajectories of three deuterons (in white) with energy >100 keV for a duration of 10 ns shown against the background plasma density. The gyro-motion of the particles is clearly evident. Bottom: The trajectory (shown in black) of a 1.01 MeV triton produced in the hot central region of the plasma. The triton escapes from the central region and becomes trapped by the **B** field near a Rayleigh-Taylor spike.

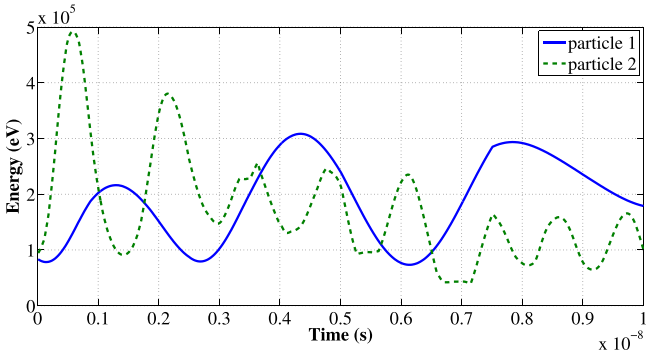

FIG. 5. The energy of two accelerated deuterons as a function of time during the stagnation phase of the gas puff. Confinement by the **B** field causes the deuteron energy to oscillate.

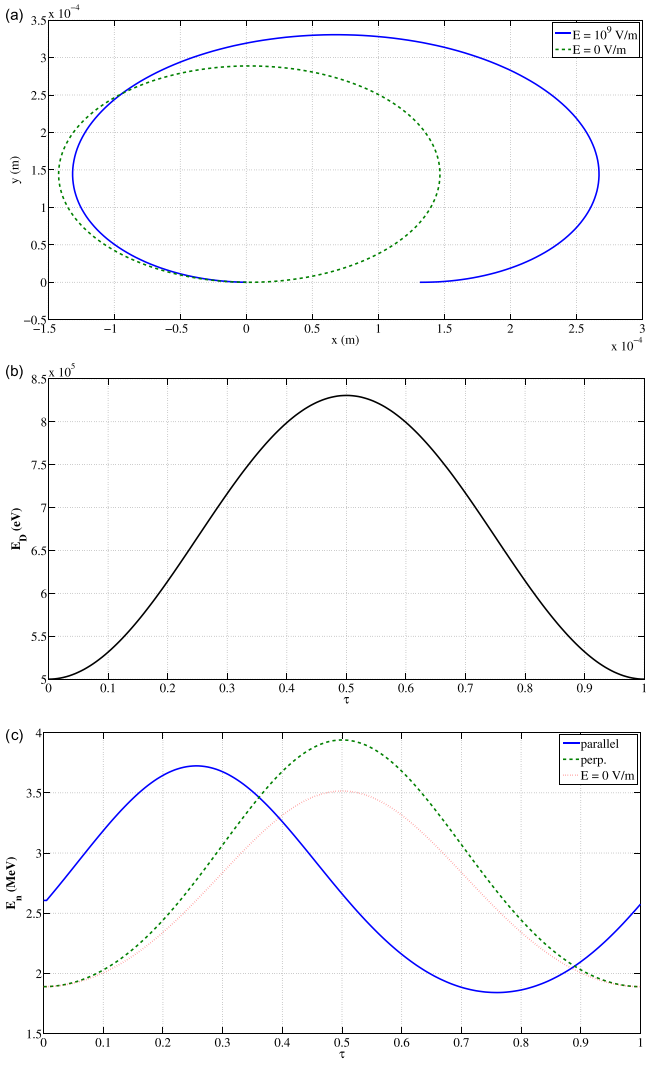

FIG. 6. Top: Gyro-orbits for 500 keV deuteron in a 10^3 T **B** field (directed out of page) with an **E** field (directed in the $+y$ direction) that is either 0 or 10^9 V m^{-1}. Middle: Variation of deuteron energy with gyro-phase for the $\mathbf{E} = 10^9$ V m^{-1} case. The peak deuteron energy is 830 keV. Bottom: Energy of neutrons emitted parallel and perpendicular to the **E** field as a function of gyro-phase. The neutron energy for the case with zero **E** field (in which emission is isotropic) is also shown. Interestingly, neutrons emitted perpendicular to the **E** field reach a higher energy than those emitted parallel to the **E** field.

neutron emitted in a given direction varies by over 2 MeV during a gyro-orbit. This magnetization effect can explain why isotropic BT spectra are observed in the simulations. The **E** field is primarily in the axial direction during the stagnation phase of the gas puff and so ions are accelerated in this direction immediately after they are created. Therefore, ions that react soon after initial acceleration will tend to produce anisotropic spectra. For ions that undergo significant nonlocal transport, the time from creation to reaction will be longer. However, ions that undergo significant nonlocal transport will become magnetically confined and so will tend to produce isotropic spectra. Therefore, the time-integrated BT spectrum emitted in the axial direction from 0 to 5 ns is shifted to higher energy than the radial spectrum. As time evolves, the contribution to the time-integrated BT spectrum from magnetically confined ions increases. Therefore, the isotropy in the time-integrated BT spectra is more pronounced in the spectrum for the 0–10 ns time period compared to the 0–5 ns time period.

The lower energy peak for the BT spectra results from the reaction kinematics, in particular, from an effect that we refer to as kinematic pile-up of neutrons emitted with large scattering angles. This effect is illustrated in Fig. 7. When a beam particle of variable energy reacts with a target particle, then the energy of the neutron emitted in the forward direction is much more sensitive to the beam particle energy than the neutron emitted in the backward direction. This is due to a trade-off that occurs between the centre of mass velocity and kinetic energy in the centre of mass frame for backward emitted neutrons.[28] As shown in Fig. 7, the effect is particularly strong for DD neutrons in which no neutron is emitted below an energy of 1.63 MeV if the target particle is

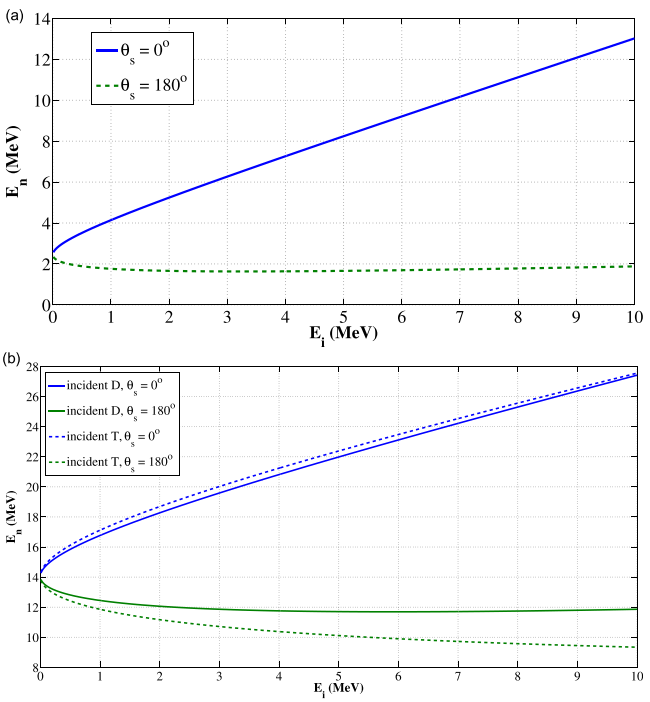

FIG. 7. The energy of neutrons emitted in the forward and backward directions when one reactant particle is incident on a stationary reactant. Top: $D(d,n)He^3$, bottom: $T(d,n)He^4$.

stationary. If the energy range of accelerated ions is on the order of a MeV or greater, then the kinematic pile-up effect outweighs the effect of the differential cross-section (which has a peak for neutrons emitted with small scattering angles), resulting in neutron spectra that have a peak at a lower energy. Neutrons emitted with a small scattering angle contribute to a long tail in the high energy portion of the spectrum. This kinematic pile-up effect can explain the BT spectrum peaks located near 2.3 MeV in Fig. 3.

We can conclude that if there is a significant yield of BT neutrons in the 15 MA gas puff, then it is likely that the BT spectra are isotropic, broad, and with a peak at an energy of less than 2.45 MeV. Therefore, the observation of isotropic neutron spectra is not a sufficient requirement for the identification of a TN yield.

Finally, the model was used to investigate the production of secondary DT neutrons that can be used as a measure of the plasma ρR.[31] In the experiments on the Z machine, copper activation diagnostics with a minimum observable neutron yield of 4×10^9 were used to search for secondary neutrons. No measurable yield was recorded, suggesting that the yield of secondary neutrons was below this value.[30] In our simulations, we model secondary neutron production by producing 1.01 MeV triton particles from DD TN fusion reactions. These triton particles are then tracked in the same way as the accelerated deuterons, and their reactivity with the background plasma is recorded. The simulation predicts a secondary neutron yield of 5×10^9, close to the threshold value of the detectors used in the experiment. From this, we infer a ρR value for the plasma of $2 \times 10^{-2}\,\mathrm{kg\,m^{-2}}$. The ρR of the simulated plasma at stagnation has a maximum value of $9 \times 10^{-3}\,\mathrm{kg\,m^{-2}}$. The discrepancy between these two values is likely due to elongated paths for some of the tritons caused by magnetization. However, an investigation of the triton dynamics suggests that the tritons are not well confined in the dense column of plasma on axis but instead escape and become magnetically trapped in regions of low plasma density. This is illustrated in Fig. 4. This is in contrast to recent results from the MagLIF project, which suggests that 1.01 MeV tritons are magnetically confined in the dense fuel region.[32]

B. 2 MA DPF

The geometry and implosion dynamics of the dense plasma focus differs significantly from the gas puff even though both devices result in similar stagnation phases. The DPF consists of a central anode column, surrounded by a cylindrical array of cathode rods. The entire chamber is then backfilled with deuterium gas. When current is initiated, breakdown occurs at the base of the anode and the current begins to flow radially. As the current increases, a current sheath moves axially along the DPF, causing a snowploughing of the deuterium gas (the rundown phase). When the current sheath reaches the end of the anode, it begins to move radially inwards along the top of the anode, resulting in a plasma pinch forming at stagnation.

For this work, we have simulated two DPFs that differ significantly in size. The first is the Gemini DPF operated by NSTec, illustrated in Fig. 8, capable of a maximum current

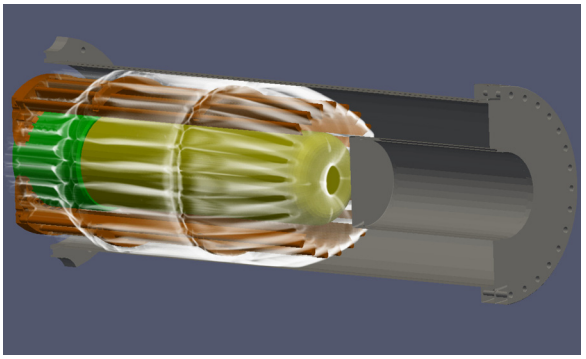

FIG. 8. An image taken from the MHD simulation of a 2 MA DPF. The DPF hardware and the plasma with density greater than the background deuterium density are shown. The image is taken during the rundown phase and shows cylindrical convergence of the plasma on the top surface of the anode as well as plasma being forced radially outwards through the cathode rods.

of 5 MA. The electrode geometry consists of an anode that is 60 cm tall with a radius of 7 cm and cathode rods located at a radius of 10 cm. We simulate an experiment in which the gas in the chamber has an initial pressure of 2.5 Torr and the peak current is 2.2 MA, with a rise-time of 5.7 μs. This device is simulated for both deuterium and deuterium-tritium gas fills allowing us to compare the production of 2.45 MeV neutrons with 14.05 MeV neutrons. MHD simulations show that the implosion dynamics is very similar for both fills. The rundown phase of the MHD simulation is shown in Fig. 8, while Fig. 9 shows plasma self-emission at the onset of stagnation. Perturbation structures that cause ions to accelerate are evident in this image.

The pulse duration for TN neutron production is approximately 250 ns, while for BT it is 350 ns. The TN yield is approximately 1.4×10^{12} neutrons for the DT simulation and 2×10^{10} neutrons for the DD simulation. The BT yield is 4×10^{13} and 3×10^{11} for DT and DD, respectively. The fact that the ratio of BT to TN yield is higher for DT than DD is likely due to the difference in reaction cross-sections, with the $T(d,n)He^4$ cross-section increasing more strongly

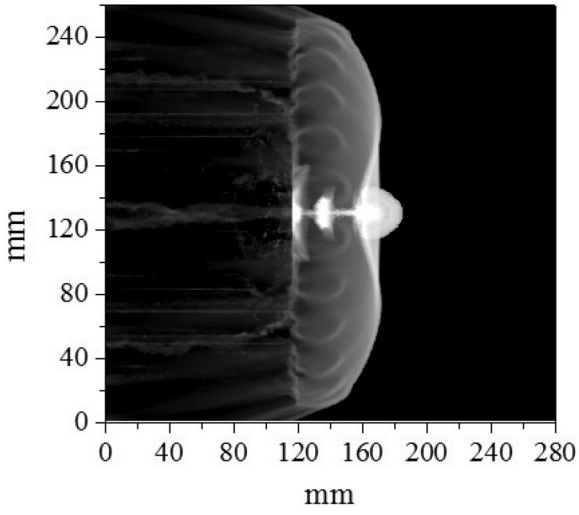

FIG. 9. A Self-emission image taken from simulations of the 2 MA DPF at the time of peak plasma compression. Significant perturbations to the stagnated plasma column are clearly visible.

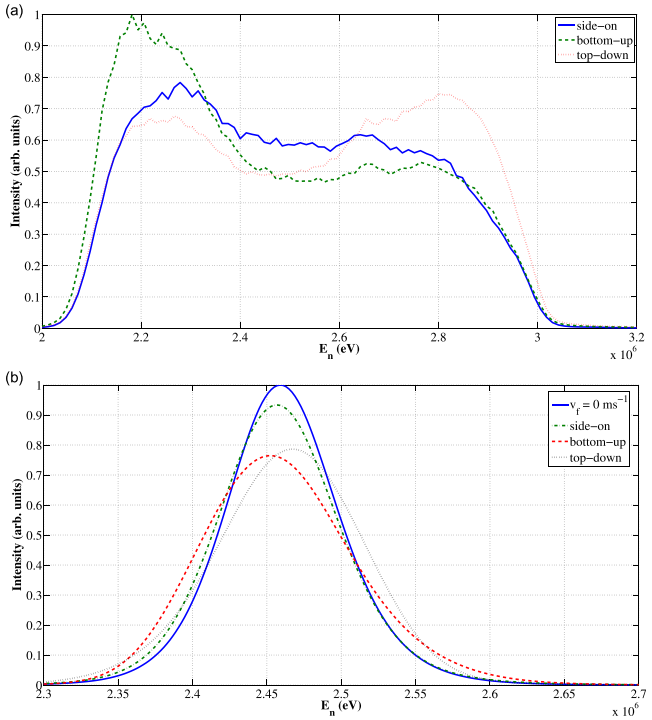

FIG. 10. Top: BT neutron spectra from a 2 MA deuterium DPF emitted in the radial and two axial directions ("bottom-up" refers to emission towards the anode). Bottom: TN neutron spectra emitted in the same directions. The TN spectrum that results when fluid motion is ignored (labelled $v_f = 0\,\mathrm{ms}^{-1}$) is also shown.

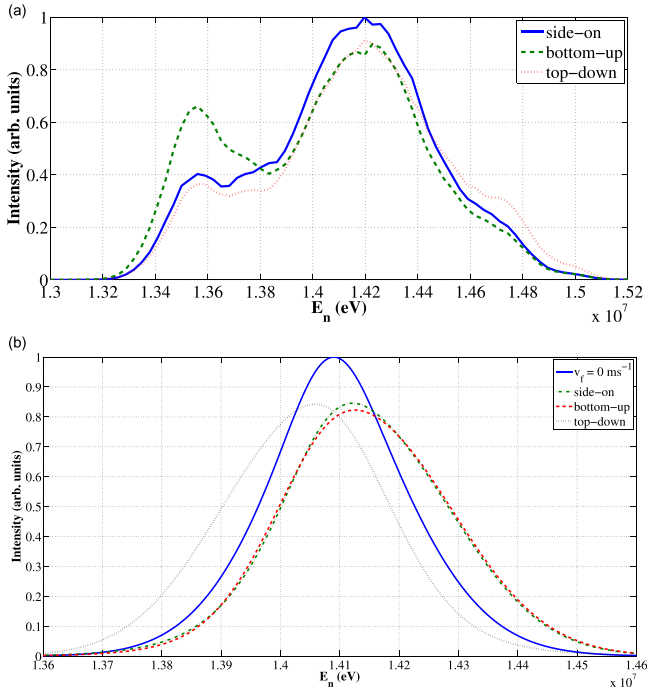

FIG. 11. Top: BT neutron spectra from a 2 MA deuterium-tritium DPF emitted in the radial and two axial directions. Bottom: TN neutron spectra emitted in the same directions.

as a function of incident energy than the $D(d,n)He^3$ cross-section for incident energies less than approximately 100 keV (as shown in Fig. 1). Since the mean energy of reacting ions is higher for BT reactions than TN reactions, this will cause the DT BT yield to outweigh the DT TN yield by a greater factor than the DD BT yield outweighs the DD TN yield.

The neutron spectra for both BT and TN neutron production are shown in Figs. 10 and 11 for the DD and DT simulations, respectively. In both cases, the effect of fluid motion on the TN spectra is evaluated by calculating the spectra with and without (spectrum labelled $v_f = 0\,\mathrm{ms}^{-1}$) fluid velocity. It is clear that the fluid motion causes a broadening and anisotropy of the TN spectra for both the DD and DT simulations. However, the TN spectra remain much narrower than the BT spectra. These TN spectra suggest that the plasma producing TN neutrons is very similar for both the DD and DT simulations. First, the effect of fluid motion is similar in both. Second, the FWHM of the TN spectra where fluid motion is ignored is 0.12 MeV for the DD simulation and 0.26 MeV for the DT simulation. These values correspond to inferred ion temperatures of 2.09 keV and 2.15 keV, respectively. The slightly higher temperature inferred from the DT spectra is to be expected since reactivity increases with temperature at a faster rate for DT than DD. This weights the DT spectra to a higher temperature than the DD spectra. Therefore, the TN spectra suggest very similar plasma dynamics for the DD and DT simulations.

However, the BT spectra for these two simulations are significantly different. The DD BT spectra have a width of approximately 0.9 MeV in every emission direction. Basic kinematics (see Subsection 1 of the Appendix) suggests that the energy range of a DT neutron is approximately twice that of a DD neutron for reactants with equal energy. Therefore, we would expect the BT spectra in the DT simulation to have a width close to 2 MeV. However, the DT neutron spectra have a width significantly less than this and are also dominated by a narrower peak region centered at approximately 14.2 MeV. The differences between these observed spectra can be explained by differences in the reaction cross-sections, in particular, the peak in the DT cross-section that occurs for incident particle energies of approximately 100 keV (as shown in Fig. 1). In both simulations, ions are accelerated to an energy range of approximately 50–250 keV. The DD cross-section increases monotonically with increasing reactant energy and so higher energy deuterons make the strongest contributions to the neutron spectrum. However, the relatively sharp peak in the DT cross-section means that ions with an energy of approximately 100 keV make the strongest contributions to the DT neutron spectrum.

C. 70 kA and 500 kA DPF

The hybrid MHD-kinetic model is also used to simulate neutron production in sub-MA DPFs designed for operation at a rate of 1 Hz or greater.[33] The electrode geometry for this DPF consists of a central anode column of radius 0.75 cm, height 2.0 cm, surrounded by 12 cathode posts at a radius of 2.5 cm. Simulations of this set-up are carried out for currents of 70 kA and 500 kA with initial deuterium densities of $2 \times 10^{-4}\,\mathrm{kg\,m}^{-3}$ and $1.53 \times 10^{-2}\,\mathrm{kg\,m}^{-3}$, respectively. In both cases, the current rise-time is 630 ns.

Details of the implosion dynamics and accelerated ion trajectories were reported in a previous publication.[34] It was shown that the stagnation phase comprised of two parts. First, a well-collimated pinch was formed on axis. This was then followed by a highly perturbed break-up of the pinch driven by the $m = 1$ instability. It was found that the majority of ions were accelerated during this break-up phase when a significant portion of the plasma surface had an orthogonal **E** field. The kinetic ion model was run for 20 ns time period during the stagnation phase. The mean energies of accelerated deuterons were 100 keV and 300 keV for the 70 kA and 500 kA DPFs, respectively. The difference in mean ion energies is due to the much stronger **E** field present in the 500 kA DPF. The effect of the **B** field was almost negligible in the 70 kA DPF. For the 500 kA, the **B** field caused some curvature of the accelerated ions, but there was little evidence of magnetic confinement of these particles.

The neutron spectra resulting from these simulations are shown in Fig. 12. In both devices, the TN yield is negligible, while the BT yield is approximately 10^6 for 70 kA and 10^8 for 500 kA. In the case of the 70 kA device, this yield is in agreement with experimental data. Comparing the spectra emitted by both devices, it is clear that the higher mean ion energy in the 500 kA device causes a greater shift in the axially emitted spectra for this device. For both devices, there is clear anisotropy of the spectra implying that majority of accelerated ions are moving in the axial-up direction. However, there are two indicators that also imply that there are significant ion populations with velocity components in the axial-down and radial directions. First, the spectra emitted in all directions have similar widths. Second, the spectra emitted in the axial-down directions have a significant tail at high neutron energies, while spectra emitted in the axial-up direction have a significant tail at low neutron energies.

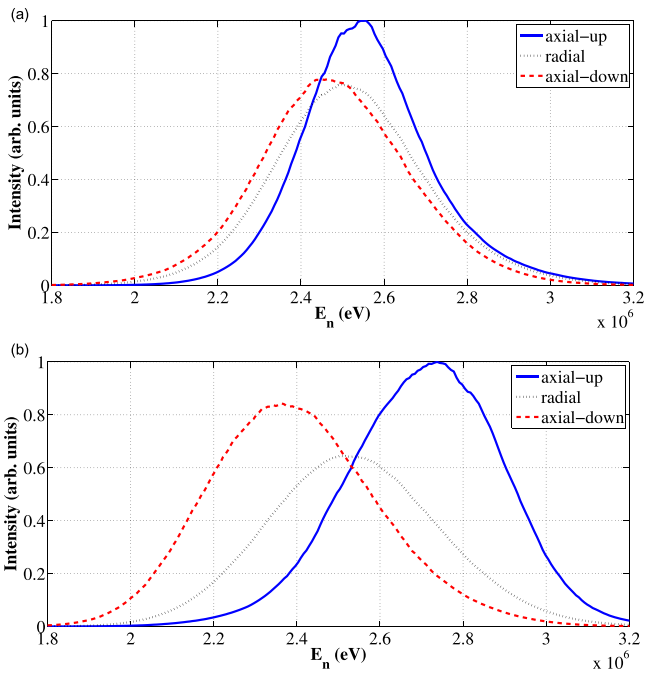

FIG. 12. Time-integrated BT neutron spectra emitted by a 70 kA (top) and 500 kA (bottom) DPF during a 20 ns time period during stagnation and break-up of the pinch column. "Axial-down" refers to emission towards the anode.

Finally, it should be noted that the mean neutron energy of 300 keV is significantly larger than would be inferred from the spectra from the 500 kA device. A 300 keV beam deuteron produces a neutron of approximately 3 MeV in the forward direction when it reacts with a stationary deuteron. The mean neutron energy in the axial-up direction is approximately 2.75 MeV. The discrepancy between these values suggests that deuterons accelerated to higher energies are less reactive. This could arise, for example, if ions accelerated to higher energies were transported to vacuum regions or regions with a low density of background plasma or if lower energy ions become magnetically confined and so have an increased effective path length in the plasma.

IV. ANALYZING FUSION NEUTRON SPECTRA

The synthetic neutron spectra shown in Sec. III are characteristic of the particular physics that we have modeled, that is, TN production in a turbulent stagnated plasma and BT production due to ion acceleration by inhomogeneous **E** and **B** fields in such a plasma. It is interesting to note that the BT spectra are qualitatively similar to experimentally observed spectra that are reported in the literature. For example, data from 2 to 3 MA deuterium gas puff experiments[35–37] show spectra that have comparable levels of anisotropy and FWHM to the BT spectra shown in Fig. 10. Similar spectra have also been reported for 2 MA DPF experiments,[38] 2 MA DPF PIC simulations,[39] and deuterated polyethylene Z-pinch experiments.[40]

Due to this similarity between the synthetic spectra here and experimental spectra in the literature, it is tempting to conclude that the same mechanisms are responsible for neutron production in the simulations and experiments. In this section, we analyze the kinetics of neutron spectra production in greater detail in order to gain some insights into the uniqueness of the spectra shown in Sec. III.

A. Thermonuclear spectra

The shape of neutron spectra resulting from homogeneous TN plasmas is well understood.[26,41,42] These spectra are isotropic with a maximum intensity at an energy that is close to the nominal neutron energy for the reaction (2.45 MeV for DD and 14.05 MeV for DT neutrons, respectively). As shown in the results of Sec. III, the FWHM of a TN spectrum is typically much smaller than the FWHM from BT spectra. For example, the FWHM of the BT spectra emitted by the 70 kA DPF (approximately 400 keV) would imply an implausibly high burn-averaged ion temperature of approximately 11 keV if these spectra were interpreted as being TN. Furthermore, the tails of a TN neutron spectrum decay exponentially, whereas BT spectra often display a much more elongated high energy tail. Therefore, it is highly unlikely that a purely TN plasma could produce neutron spectra similar to the BT spectra shown in Sec. III.

B. Thermonuclear spectra broadened by bulk fluid motion

Recent theoretical work has suggested that bulk fluid motion of a TN plasma can have a noticeable broadening effect on neutron spectrum width in inertial confinement fusion,[42–44] potentially causing an erroneously high ion temperature to be inferred from the spectrum width. This effect was included in the simulations of the 15 MA gas puff and 2 MA DPF. As shown in Figs. 2, 10, and 11, it does alter the TN spectrum. However, these spectra remain very different from the BT spectra produced by the simulations. Furthermore, we can use more basic calculations to show that, in general, a BT spectrum can be distinguished from a fluid-broadened spectrum.

We first consider a uniform, cylindrical plasma shell converging on axis with a given radial velocity. The equation governing this spectrum is given in Subsection 2 of the Appendix and is plotted in Fig. 13 for a number of fluid velocities as well as the FWHM of the spectrum as a function of the fluid velocity. From fluid velocities of approximately $10^5\,\mathrm{ms}^{-1}$ upwards, the radially emitted spectrum is noticeably broader than the TN spectrum in which fluid broadening is not considered ($v_f = 0\,\mathrm{ms}^{-1}$). However, the results show that in order for the width of the radially emitted spectrum to be comparable with typical widths of BT spectra, the fluid velocity needs to be close to or greater than the implosion velocity of the device. Such a plasma will necessarily have a low ion temperature and low reactivity. Furthermore, the neutron spectrum emitted axially is largely unaffected by this fluid motion and so will be much narrower than the radial spectrum.

The second fluid model that we consider is axial flow of a TN emitting plasma. If we consider the spectra produced by the 500 kA DPF shown in Fig. 12, the question arises of whether fluid flow in the axial-up direction could produce spectra similar to the observed BT spectra. Certainly, such a fluid flow would lead to a similar anisotropy of the spectra. However, it is straightforward to calculate that a fluid velocity of $1.25 \times 10^6\,\mathrm{ms}^{-1}$ in the axial-up direction would be required to shift the peak of the axial-up spectrum from 2.45 MeV to 2.74 MeV, while a fluid velocity of $4 \times 10^5\,\mathrm{ms}^{-1}$ would be required to shift the axial-down spectrum to 2.36 MeV. In addition, we would expect the radial spectrum in this example to be much narrower if fluid motion was responsible for the shifts in the axially emitted spectra.

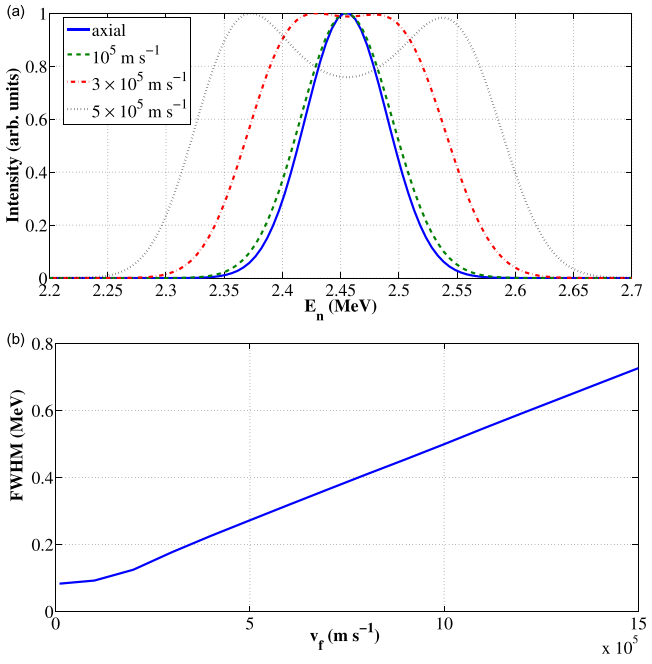

FIG. 13. Top: The DD neutron spectrum emitted radially for a number of cylindrically convergent fluid flows of the given velocities. The axially emitted spectrum is also shown here. Bottom: The FWHM of the radially emitted spectra as a function of fluid velocity. The ion temperature is 1 keV.

In general, it seems that attempting to fit BT spectra with fluid-broadened TN spectra requires the introduction of values of the fluid velocity and ion temperature than are implausible given the implosion dynamics of the system.

C. Magnetization as a cause of isotropic beam-target spectra

In Sec. III A, it was shown that magnetization of the accelerated ions resulted in isotropic BT spectra for the 15 MA gas puff. The question then arises that if a dense Z-pinch emits isotropic neutron spectra with features such as width or the peak energy that eliminate the possibility of a TN source, then what mechanisms aside from magnetization could be responsible?

Isotropic BT spectra such as those shown in Fig. 3 can be caused by one of two effects, namely, (i) either ions are accelerated isotropically or (ii) there is a mechanism by which anisotropically accelerated ions become isotropic.

Regarding the first of these, the lack of spherical symmetry in the imploding Z-pinch makes isotropic acceleration unlikely. It is still possible that a sufficiently perturbed implosion could lead to a turbulent stagnation phase with an **E** field that isotropically accelerates ions. However, the scale length of such an **E** field is likely to be very small in comparison with the pinch length, making it difficult to accelerate ions to high energies.

Regarding the second effect, aside from magnetization, processes that have an isotropizing effect on accelerated ions include collisionality. However, the effect of collisions on a beam is to cause it to evolve into a Maxwellian distribution. Therefore, we would expect the resulting isotropic neutron spectrum to be TN.

Therefore, we conclude that magnetization of accelerated ions is the most likely explanation for isotropic BT spectra, particularly when the ions are accelerated to high energies (as evidenced by high energy tails of these isotropic spectra). It is worth noting that recent experimental results from deuterium gas puffs suggested that magnetization effects may be present for neutrons with energies greater than 10 MeV.[45]

D. Spectra with a lower energy peak

If we can eliminate fluid motion as a cause, then there are two mechanisms for producing BT spectra with a peak intensity at a lower energy than the nominal neutron energy. In both cases, kinematic pile-up (illustrated in Fig. 7) is important.

The first mechanism is anisotropic motion of the accelerated ions. In this case, the spectrum with a peak at lower

energy should be accompanied by a spectrum emitted in the opposite direction with a peak at higher energy. If the energy range of the ions extends above 1 MeV, then the kinematic pile-up effect can become significant, causing the peak intensity of the lower energy spectrum to be greater than the higher energy spectrum even though the yield of the higher energy spectrum would still be greater.

The second mechanism is isotropic motion of the accelerated ions, caused, for example, by magnetization. The emitted spectra are isotropic and kinematic pile-up is the direct cause of the lower energy peak, as is the case in Fig. 3. The broader the range of energies of the accelerated ions, then the greater the intensity of the spectrum peak relative to the high energy tail component. Such a neutron spectrum will also have a long high energy tail causing the mean neutron energy to remain close to the nominal neutron energy.

Because of kinematic differences between the two reactions, these features will be sharper for the DD spectrum than the DT spectrum. In particular, Fig. 7 shows that no neutrons can be emitted with an energy of less than 1.63 MeV when a beam deuteron reacts with a stationary deuteron. In the gas puff spectra shown in Fig. 3, neutrons with an energy lower than this value are produced. This is due to thermal broadening caused by the finite ion temperature of the target deuterons. Experimental data also suggest that neutron scattering can also be a source of neutrons in this region.[37,38]

E. Beam-target spectrum width

A quantitative relationship between the width of BT spectra and some physical parameters of the system is desirable, analogous to that between spectrum width and ion temperature for TN reactions. In the case of uniaxial acceleration of the ions, such a relationship would be obtainable since there is a direct correlation between the energy range of accelerated ions and the spectrum width in the forward direction. However, the complex ion trajectories, magnetization of ions, and kinematic pile-up effect mean that it is difficult to relate the spectra widths to the physical conditions.

It should be noted that a number of authors have shown how power-law energy distributions of plasma ions can produce neutron spectrum with large widths, similar to the BT spectra reported here.[40,46–48] However, in order to account for anisotropic neutron spectra, parameters defining the angular variation of the ion distribution function must also be introduced. It is not yet known how to relate the parameters used for such a fitting to the physical mechanisms of neutron production.[46] Future work will investigate if the ion acceleration mechanism described in this paper results in a power-law spectrum and if this spectrum can be related to the pinch conditions at stagnation.

F. Combined beam-target and TN spectra

Previous computational work[6] has suggested that for 7–15 MA deuterium Z-pinches, approximately equal amounts of BT and TN neutrons are produced. The results contained in this paper suggest that if this is the case, then it should be identifiable in the emitted neutron spectra. In all the devices that we have simulated, the TN spectrum is so narrow in comparison with the BT that if the yields were comparable, then the TN spectrum component would be visible as an intense narrow peak in a much broader BT spectrum. An example of this is shown in Fig. 14. Therefore, if a broad neutron spectrum is measured without a narrow TN peak, we can estimate an upper limit for R_y, the yield ratio of TN to BT neutrons.

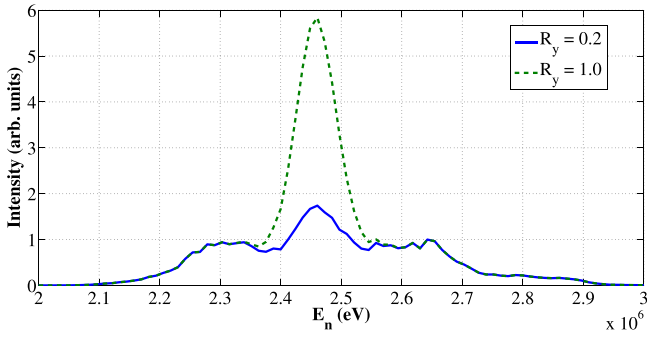

FIG. 14. Combined BT and TN neutron spectra in the radial direction for the 2 MA deuterium DPF for a 20 ns period during peak emission. The variable R_y refers to the ratio of TN to BT yield. The spectrum labelled $R_y = 0.2$ is the result of the simulation, while the $R_y = 1.0$ spectrum has an artificially scaled up yield.

V. SUMMARY AND CONCLUSIONS

Recent experimental results from the MagLIF project[49] have highlighted the importance of neutron spectroscopy diagnostics. In these experiments, DD spectra were used to measure the ion temperature[50] (there was no evidence of BT neutrons in this data), while the DT neutron spectra from secondary neutrons[32] were used to infer the level of magnetization of the deuterium plasma. The aim of this paper is to show that neutron spectroscopy has the potential to be a powerful diagnostic in other Z-pinch regimes. In particular, we make the following specific conclusions regarding the BT neutron spectra produced in Z-pinches

(1) The TN spectrum in a Z-pinch is susceptible to broadening due to fluid motion of the emitting plasma. However, the magnitude of the shifts and widths of BT spectra means that BT spectra should still be distinguishable from TN spectra. Also, the large width of BT spectra means that if there was a TN source present with a comparable yield to the BT yield, then it is likely that the TN neutrons will cause a narrow peak to be present in the neutron spectrum.
(2) BT spectra can have a peak at an energy lower than the nominal energy value of the reaction (i.e., less than 2.45 MeV and 14.05 MeV for DD and DT neutrons, respectively). This feature can be due to the reaction kinematics (and not just neutron scattering) and can occur even when beam particles are moving isotropically.
(3) BT spectra can be isotropic even if the initial acceleration mechanism is highly anisotropic, due to magnetization of the accelerated ions.
(4) Differences in the cross-sections for the $D(t,n)He^4$ and $D(d,n)He^3$ reactions mean that a comparison of the DD and DT neutron spectra produced from the same device has the potential to act as a diagnostic of the

accelerated ions. In particular, the fraction of ions with an energy greater than the energy corresponding to the peak of the $D(t,n)He^4$ reaction cross-section will be a function of the ratio of widths of DT and DD neutron spectra.

Further work is required to make the above observations quantifiable and also to examine how they are affected by experimental realities such as neutron scattering. The issue of magnetization of accelerated ions is particularly interesting since this causes a large increase in the path length of ions in the background plasma and could potentially lead to a significant increase in the BT yield. However, it may also be the case that the currents required to cause ion magnetization are also large enough to make the TN mechanism the dominant neutron production mechanism, as our results here suggested. The shape of emitted neutron spectra can help to resolve such questions.

Finally, we note that the above results have been achieved using a particular model for ion acceleration in an MHD plasma that does not include feedback from the kinetic ions to the MHD plasma. The effect of this feedback on neutron yields and spectra will be addressed in future work.

ACKNOWLEDGMENTS

The authors would like to thank Daniel Lowe and Chris Hagen of NSTec for providing data on the Gemini DPF. The results reported in this paper were obtained using the UK National Supercomputing Service ARCHER and the Imperial College supercomputer CX1. The authors also acknowledge financial support from AWE.

APPENDIX: SUPPORTING CALCULATIONS FOR NEUTRON SPECTRA

1. Energy range of emitted neutrons

Consider a deuteron and triton of equal energies reacting with a stationary deuteron. The triton momentum is $m_t\mathbf{v}$ and the deuteron momentum is $\sqrt{m_t m_d}\mathbf{v}$. The energy of a neutron emitted by either of these reactions is given by

$$E_n = \frac{1}{2} m_n (\mathbf{v_{cm}} + \mathbf{u_n})^2, \tag{A1}$$

where $\mathbf{v_{cm}}$ is the centre of mass velocity of the reactants and $\mathbf{u_n}$ is the neutron velocity of the centre of mass frame, the magnitude of which is given by

$$u_n = \frac{2}{\eta}\sqrt{Q + \frac{1}{2}\mu v_r^2}, \tag{A2}$$

$$\eta = \frac{m_n(m_n + m_4)}{m_4}, \tag{A3}$$

where v_r and μ are the relative velocity and reduced mass of the reactants, respectively, Q is the Q-value of the reaction, and m_4 is the mass of a He^3 (He^4) nucleus for the DD (DT) reaction. Equation (A1) can be used to calculate the maximum and minimum neutron energy

$$E_n = \frac{1}{2} m_n (v_{cm} \pm u_n)^2. \tag{A4}$$

This expression is plotted in Fig. 7, and from it, we obtain the energy range of neutrons emitted by a reaction

$$E_n^{max} - E_n^{min} = 2 m_n v_{cm} u_n. \tag{A5}$$

The ratio of this energy range for DT and DD neutrons may be expressed as

$$\frac{2\sqrt{m_t m_d}}{m_t + m_d}\frac{\eta_{DT}}{\eta_{DD}}\frac{\sqrt{Q_{DT} + \frac{m_d}{m_t + m_d}E_i}}{\sqrt{Q_{DD} + \frac{1}{2}E_i}} \approx 0.92\frac{\sqrt{Q_{DT} + \frac{m_d}{m_t + m_d}E_i}}{\sqrt{Q_{DD} + \frac{1}{2}E_i}}. \tag{A6}$$

This expression has a value of 2.13 for $E_i = 50\,\text{keV}$ and 2.07 for $E_i = 500\,\text{keV}$, suggesting that we would expect a DT neutron spectrum to be approximately twice as wide as a DD neutron spectrum produced under similar conditions. As discussed in Sec. III B, differences in the cross-sections for the two reactions can alter this prediction.

2. Neutrons emitted by an imploding cylindrical shell

An expression was previously derived for the neutron spectrum emitted by a spherical plasma shell of uniform temperature imploding radially with a given velocity.[42] The same procedure can be used in cylindrical geometry to obtain the spectrum emitted by a uniform, cylindrical plasma shell converging onto the axis with a given velocity. The neutron spectrum emitted in the radial direction by such a cylinder is given by

$$R_\perp^{cyl}(\mathbf{v_n})\frac{n_1 n_2}{1+\delta_{12}}\eta\frac{\sqrt{m_1 m_2}}{(2\pi T)^2} \times \int_{v_Q}^{\infty}\zeta^2\sigma(\zeta)\exp\left(-\frac{\mu}{2T}\zeta^2\right)\left[F^-(u) - F^+(u)\right]du, \tag{A7}$$

where

$$F^{\pm}(u) = \int_0^{\pi}\frac{1}{\sqrt{v_n^2 + v_f^2 - 2v_n v_f\cos\phi_f}} \times \exp\left(-\alpha\left(\sqrt{v_n^2 + v_f^2 - 2v_n v_f\cos\phi_f} \pm u\right)^2\right)d\phi_f, \tag{A8}$$

and

$$\zeta = \sqrt{\frac{2}{\mu}\left(\frac{\eta}{2}u^2 - Q\right)},$$

$$\alpha = (m_1 + m_2)/2T,$$

$$v_Q = \sqrt{2\frac{Q}{\eta}}.$$

The notation used is as follows: T is the ion temperature, v_n is neutron velocity, v_f is fluid velocity, and n_1, n_2 are the reactant particle number densities. Other notation is as defined in Subsection 1 of the Appendix. Equation (A7) is plotted in Fig. 13.

[1]O. A. Anderson, W. R. Baker, S. A. Colgate, J. Ise, and R. V. Pyle, "Neutron production in linear deuterium pinches," Phys. Rev. **110**, 1375–1387 (1958).

[2]M. Krishnan, "The dense plasma focus: A versatile dense pinch for diverse applications," IEEE Trans. Plasma Sci. **40**, 3189–3221 (2012).

[3]S. Lee, "Neutron yield saturation in plasma focus: A fundamental cause," Appl. Phys. Lett. **95**, 151503 (2009).

[4]C. A. Coverdale, C. Deeney, A. L. Velikovich, R. W. Clark, Y. K. Chong, J. Davis, J. Chittenden, C. L. Ruiz, G. W. Cooper, A. J. Nelson, J. Franklin, P. D. LePell, J. P. Apruzese, J. Levine, J. Banister, and N. Qi, "Neutron production and implosion characteristics of a deuterium gas-puff z pinch," Phys. Plasmas (1994-present) **14**, 022706 (2007).

[5]A. L. Velikovich, R. W. Clark, J. Davis, Y. K. Chong, C. Deeney, C. A. Coverdale, C. L. Ruiz, G. W. Cooper, A. J. Nelson, J. Franklin, and L. I. Rudakov, "Z-pinch plasma neutron sources," Phys. Plasmas (1994-present) **14**, 022701 (2007).

[6]D. R. Welch, D. V. Rose, C. Thoma, R. E. Clark, C. B. Mostrom, W. A. Stygar, and R. J. Leeper, "Kinetic simulation of thermonuclear-neutron production by a 10^7a deuterium z pinch," Phys. Plasmas (1994-present) **17**, 072702 (2010).

[7]D. Klir, V. Kokshenev, P. Kubes, A. Labetsky, M. Paduch, K. Rezac, and A. Shishlov, "Search for drive parameter of neutron-optimized z-pinches and dense plasma foci," IEEE Trans. Plasma Sci. **41**, 3129–3134 (2013).

[8]M. J. Bernstein and G. G. Comisar, "Neutron energy and flux distributions from a crossed field acceleration model of plasma focus and z pinch discharges," Phys. Fluids (1958–1988) **15**, 700–707 (1972).

[9]U. Jager and H. Herold, "Fast ion kinetics and fusion reaction mechanism in the plasma focus," Nucl. Fusion **27**, 407 (1987).

[10]D. D. Ryutov, M. S. Derzon, and M. K. Matzen, "The physics of fast z pinches," Rev. Mod. Phys. **72**, 167–223 (2000).

[11]M. G. Haines, "A review of the dense z-pinch," Plasma Phys. Controlled Fusion **53**, 093001 (2011).

[12]R. Deutsch and W. Kies, "Ion acceleration and runaway in dynamical pinches," Plasma Phys. Controlled Fusion **30**, 263 (1988).

[13]M. G. Haines, "Ion beam formation in an m = 0 unstable z pinch," Nucl. Instrum. Methods Phys. Res. **207**, 179–185 (1983).

[14]A. Schmidt, V. Tang, and D. Welch, "Fully kinetic simulations of dense plasma focus," Phys. Rev. Lett. **109**, 205003 (2012).

[15]A. Schmidt, A. Link, D. Welch, J. Ellsworth, S. Falabella, and V. Tang, "Comparisons of dense-plasma-focus kinetic simulations with experimental measurements," Phys. Rev. E **89**, 061101 (2014).

[16]D. R. Welch, D. V. Rose, C. Thoma, R. E. Clark, C. B. Mostrom, W. A. Stygar, and R. J. Leeper, "Kinetic simulations of a deuterium-tritium z pinch with $>10^{16}$ neutron yield," Phys. Plasmas (1994-present) **18**, 056303 (2011).

[17]F. Castillo, J. J. E. Herrera, J. Rangel, M. Milanese, R. Moroso, J. Pouzo, J. I. Golzarri, and G. Espinosa, "Isotropic and anisotropic components of neutron emissions at the fn-ii and paco dense plasma focus devices," Plasma Phys. Controlled Fusion **45**, 289 (2003).

[18]F. Castillo, J. J. E. Herrera, I. Gamboa, J. Rangel, J. I. Golzarri, and G. Espinosa, "Angular distribution of fusion products and x rays emitted by a small dense plasma focus machine," J. Appl. Phys. **101**, 013303 (2007).

[19]M. V. Roshan, R. S. Rawat, A. Talebitaher, P. Lee, and S. V. Springham, "Neutron and high energy deuteron anisotropy investigations in plasma focus device," Phys. Plasmas **16**, 053301 (2009).

[20]*Presented at the International Conference on Progress and Applications of Plasma Focus Research*, edited by R. B. Spielman, and G. T. Baldwin, G. Cooper, Hoboken, NJ, 27 May 1994.

[21]D. R. Welch, D. V. Rose, R. E. Clark, C. B. Mostrom, W. A. Stygar, and R. J. Leeper, "Fully kinetic particle-in-cell simulations of a deuterium gas puff *z* pinch," Phys. Rev. Lett. **103**, 255002 (2009).

[22]C. A. Jennings, M. E. Cuneo, E. M. Waisman, D. B. Sinars, D. J. Ampleford, G. R. Bennett, W. A. Stygar, and J. P. Chittenden, "Simulations of the implosion and stagnation of compact wire arrays," Phys. Plasmas **17**, 092703 (2010).

[23]A. Ciardi, S. V. Lebedev, A. Frank, E. G. Blackman, J. P. Chittenden, C. J. Jennings, D. J. Ampleford, S. N. Bland, S. C. Bott, J. Rapley, G. N. Hall, F. A. Suzuki-Vidal, A. Marocchino, T. Lery, and C. Stehle, "The evolution of magnetic tower jets in the laboratory," Phys. Plasmas (1994-present) **14**, 056501 (2007).

[24]M. Sherlock, "A Monte-Carlo method for coulomb collisions in hybrid plasma models," J. Comput. Phys. **227**, 2286–2292 (2008).

[25]S. Vickers, "Particle in cell and hybrid simulations of the Z double-post-hole convolute cathode plasma evolution and dynamics," Ph.D. thesis (Imperial College London, 2013).

[26]B. Appelbe and J. Chittenden, "Relativistically correct DD and DT neutron spectra," High Energy Density Phys. **11**, 30–35 (2014).

[27]B. Appelbe, "Nuclear fusion reaction kinetics and ignition processes in Z pinches," Ph.D. thesis (Imperial College London, 2011).

[28]B. Appelbe and J. Chittenden, "Quasi-monoenergetic spectra from reactions in a beam-target plasma," Phys. Plasmas (1994-present) **19**, 073115 (2012).

[29]M. B. Chadwick, P. Obložinský, M. Herman, N. M. Greene, R. D. McKnight, D. L. Smith, P. G. Young, R. E. Macfarlane, G. M. Hale, S. C. Frankle, A. C. Kahler, T. Kawano, R. C. Little, D. G. Madland, P. Moller, R. D. Mosteller, P. R. Page, P. Talou, H. Trellue, M. C. White, W. B. Wilson, R. Arcilla, C. L. Dunford, S. F. Mughabghab, B. Pritychenko, D. Rochman, A. A. Sonzogni, C. R. Lubitz, T. H. Trumbull, J. P. Weinman, D. A. Brown, D. E. Cullen, D. P. Heinrichs, D. P. McNabb, H. Derrien, M. E. Dunn, N. M. Larson, L. C. Leal, A. D. Carlson, R. C. Block, J. B. Briggs, E. T. Cheng, H. C. Huria, M. L. Zerkle, K. S. Kozier, A. Courcelle, V. Pronyaev, and S. C. van der Marck, "ENDF/B-VII.0: Next generation evaluated nuclear data library for nuclear science and technology," Nucl. Data Sheets **107**, 2931–3060 (2006).

[30]C. A. Coverdale, C. Deeney, A. L. Velikovich, J. Davis, R. W. Clark, Y. K. Chong, J. Chittenden, S. Chantrenne, C. L. Ruiz, G. W. Cooper, A. J. Nelson, J. Franklin, P. D. LePell, J. P. Apruzese, J. Levine, and J. Banister, "Deuterium gas-puff Z-pinch implosions on the Z accelerator," Phys. Plasmas **14**, 056309 (2007).

[31]M. D. Cable and S. P. Hatchett, "Neutron spectra from inertial confinement fusion targets for measurement of fuel areal density and charged particle stopping powers," J. Appl. Phys. **62**, 2233–2236 (1987).

[32]P. F. Schmit, P. F. Knapp, S. B. Hansen, M. R. Gomez, K. D. Hahn, D. B. Sinars, K. J. Peterson, S. A. Slutz, A. B. Sefkow, T. J. Awe, E. Harding, C. A. Jennings, G. A. Chandler, G. W. Cooper, M. E. Cuneo, M. Geissel, A. J. Harvey-Thompson, M. C. Herrmann, M. H. Hess, O. Johns, D. C. Lamppa, M. R. Martin, R. D. McBride, J. L. Porter, G. K. Robertson, G. A. Rochau, D. C. Rovang, C. L. Ruiz, M. E. Savage, I. C. Smith, W. A. Stygar, and R. A. Vesey, "Understanding fuel magnetization and mix using secondary nuclear reactions in magneto-inertial fusion," Phys. Rev. Lett. **113**, 155004 (2014).

[33]B. L. Bures, C. James, M. Krishnan, and R. Adler, "Application of an impedance matching transformer to a plasma focus," Rev. Sci. Instrum. **82**, 103506 (2011).

[34]B. Appelbe and J. Chittenden, "Understanding neutron production in the deuterium dense plasma focus," AIP Conf. Proc. **1639**, 9–14 (2014).

[35]D. Klir, A. V. Shishlov, V. A. Kokshenev, P. Kubes, A. Y. Labetsky, K. Rezac, J. Cikhardt, F. I. Fursov, B. M. Kovalchuk, J. Kravarik, N. E. Kurmaev, N. A. Ratakhin, O. Sila, and J. Stodulka, "Characterization of neutron emission from mega-ampere deuterium gas puff z-pinch at microsecond implosion times," Plasma Phys. Controlled Fusion **55**, 085012 (2013).

[36]D. Klir, J. Kravarik, P. Kubes, K. Rezac, S. Ananev, Y. Bakshaev, P. I. Blinov, A. Chernenko, E. Kazakov, V. D. Korolev, G. Ustroev, L. Juha, J. Krasa, and A. Velyhan, "Neutron energy distribution function reconstructed from time-of-flight signals in deuterium gas-puff z-pinch," IEEE Trans. Plasma Sci. **37**, 425–432 (2009).

[37]D. Klir, A. V. Shishlov, P. Kubes, K. Rezac, F. I. Fursov, V. A. Kokshenev, B. M. Kovalchuk, J. Kravarik, N. E. Kurmaev, A. Y. Labetsky, and N. A. Ratakhin, "Deuterium gas puff z-pinch at currents of 2 to 3 mega-ampere," Phys. Plasmas (1994-present) **19**, 032706 (2012).

[38]D. Klir, P. Kubes, M. Paduch, T. Pisarczyk, T. Chodukowski, M. Scholz, Z. Kalinowska, B. Bienkowska, L. Karpinski, J. Kortanek, J. Kravarik, K. Rezac, I. Ivanova-Stanik, K. Tomaszewski, and E. Zielinska, "Search for thermonuclear neutrons in a mega-ampere plasma focus," Plasma Phys. Controlled Fusion **54**, 015001 (2012).

[39]A. Schmidt, A. Link, D. Welch, B. T. Meehan, V. Tang, C. Halvorson, M. May, and E. C. Hagen, "Fully kinetic simulations of megajoule-

scale dense plasma focus," Phys. Plasmas (1994-present) **21**, 102703 (2014).
[40]Y. Bakshaev, V. Bryzgunov, V. Vikhrev, I. Volobuev, S. Danko, E. Kazakov, V. Korolev, D. Klr, A. Mironenko-Marenkov, V. Pimenov, E. Smirnova, and G. Ustroev, "Generation and anisotropy of neutron emission from a condensed z-pinch," Plasma Phys. Rep. **40**, 437–450 (2014).
[41]H. Brysk, "Fusion neutron energies and spectra," Plasma Phys. **15**, 611 (1973).
[42]B. Appelbe and J. Chittenden, "The production spectrum in fusion plasmas," Plasma Phys. Controlled Fusion **53**, 045002 (2011).
[43]T. J. Murphy, "The effect of turbulent kinetic energy on inferred ion temperature from neutron spectra," Phys. Plasmas (1994-present) **21**, 072701 (2014).
[44]S. Taylor, B. Appelbe, N. P. Niasse, and J. P. Chittenden, "Effect of perturbations on yield in ICF targets 4 3d hydro simulations," EPJ Web Conf. **59**, 04009 (2013).
[45]D. Klir, P. Kubes, K. Rezac, J. Cikhardt, J. Kravarik, O. Sila, A. V. Shishlov, B. M. Kovalchuk, N. A. Ratakhin, V. A. Kokshenev, A. Y. Labetsky, R. K. Cherdizov, F. I. Fursov, N. E. Kurmaev, G. N. Dudkin, B. A. Nechaev, V. N. Padalko, H. Orcikova, and K. Turek, "Efficient neutron production from a novel configuration of deuterium gas-puff," Phys. Rev. Lett. **112**, 095001 (2014).
[46]P. F. Knapp, D. B. Sinars, and K. D. Hahn, "Diagnosing suprathermal ion populations in z-pinch plasmas using fusion neutron spectra," Phys. Plasmas (1994-present) **20**, 062701 (2013).
[47]V. Vikhrev and A. Mironenko-Marenkov, "On the spectrum of z-pinch plasma neutrons," Plasma Phys. Rep. **38**, 225–234 (2012).
[48]V. Vikhrev and V. Korolev, "Neutron generation from z-pinches," Plasma Phys. Rep. **33**, 356–380 (2007).
[49]S. A. Slutz, M. C. Herrmann, R. A. Vesey, A. B. Sefkow, D. B. Sinars, D. C. Rovang, K. J. Peterson, and M. E. Cuneo, "Pulsed-power-driven cylindrical liner implosions of laser preheated fuel magnetized with an axial field," Phys. Plasmas (1994-present) **17**, 056303 (2010).
[50]M. R. Gomez, S. A. Slutz, A. B. Sefkow, D. B. Sinars, K. D. Hahn, S. B. Hansen, E. C. Harding, P. F. Knapp, P. F. Schmit, C. A. Jennings, T. J. Awe, M. Geissel, D. C. Rovang, G. A. Chandler, G. W. Cooper, M. E. Cuneo, A. J. Harvey-Thompson, M. C. Herrmann, M. H. Hess, O. Johns, D. C. Lamppa, M. R. Martin, R. D. McBride, K. J. Peterson, J. L. Porter, G. K. Robertson, G. A. Rochau, C. L. Ruiz, M. E. Savage, I. C. Smith, W. A. Stygar, and R. A. Vesey, "Experimental demonstration of fusion-relevant conditions in magnetized liner inertial fusion," Phys. Rev. Lett. **113**, 155003 (2014).